This is the peer reviewed version of the following article: Kearney, M.R. (2019), MicroclimOz – A microclimate data set for Australia, with example applications. *Austral Ecology*, Vol. 44, Iss. 3, Pp 534-544, which has been published in final form at

https://doi.org/10.1111/aec.12689

microclimOz – a microclimate data set for Australia, with example applications

Michael R. Kearney

School of BioSciences, The University of Melbourne, Victoria 3010

Abstract

Many problems in pure and applied ecology require the quantification of above and below ground microclimates. Here I describe a data set of hourly microclimates for the Australian continent, simulated from the years 1990 to 2017 across a grid of 1893 locations ~60 km apart. The data were generated with the NicheMapR microclimate model, driven by 0.05° gridded daily meteorological forcing data (air temperature, wind speed, humidity, cloud cover, rainfall), 0.025° elevation and 0.008° soil texture data. The above ground microclimate variables include horizontal plane solar radiation, solar zenith angle, sky temperature (from which down-welling longwave radiation can be computed), air temperature, relative humidity and wind speed at 1 cm and 120 cm height, and snow depth. The below ground variables include soil temperature, pore humidity, soil moisture and soil water potential for 0, 2.5, 5, 10, 15, 20, 30, 50, 100 and 200 cm below ground. The computations are for four shade levels (0, 50, 70 and 90%). The data set can be used for a wide variety of applications, including the computation of heat and water budgets of organisms, the potential for vegetation growth, and the computation of stress and growth indices. The use of daily forcing data also allows assessments of the consequences of extreme events including heat waves. Example applications are provided for computing plant growth potential, grasshopper egg development, lizard body temperature and mammalian energy and water requirements.

Key words: microclimate, NicheMapR, mechanistic niche modelling, soil temperature, soil moisture, biophysical ecology

Introduction

Microclimates are the environments experienced by organisms; in terrestrial environments they are typically the 'climates' near the ground or beneath it (Geiger 1950; Bramer *et al.* 2018; Kearney 2018). Increasingly, ecologists are in need of microclimatic data to make mechanistic connections between climatic and phenotypic variability (Bennie *et al.* 2014; Bramer *et al.* 2018). At one extreme, microclimatic variables can be used to solve energy and mass budgets for organisms (Porter and Gates 1969; Kearney, Munns, *et al.* 2018) and thereby estimate their body temperature (and hence biological rates) and water loss (and hence hydration state). At the other extreme, microclimatic data can be used to derive descriptive indices of habitat suitability (Varner and Dearing 2014).

There is a growing set of computational tools for calculating different aspects of microclimates and mesoclimates (Bennie *et al.* 2008; Ashcroft and Gollan 2012; Levy *et al.* 2016; Kearney and Porter 2017; Maclean *et al.* 2018). Modelled microclimatic data sets have also been developed at a global scale (Kearney, Isaac, *et al.* 2014) and for North America (Levy *et al.* 2016). Here I present a comprehensive microclimate data set for Australia, computed using the recently released NicheMapR microclimate model (Kearney and Porter 2017). This model has been extensively tested for its ability to predict both soil temperature (Kearney, Shamakhy, *et al.* 2014) and soil moisture (Kearney and Maino 2018) across Australia, with accuracy to within 10% of measurement values. A data set of microclimatic output from this model would thus be valuable for a wide range of pure and applied problems in ecology, conservation, agriculture, health and pest management in the Australian context.

There are substantial computational and storage challenges to producing microclimatic data sets; microclimates must be provided on fine (at least hourly) temporal scales to be biologically relevant, and they change strongly through space on the scale of centimetres. The approach taken here is to provide simulated microclimate data at high temporal resolution based on long-term historical (daily) forcing data, at a sufficiently large sample of sites to be able to make coarse inferences of distribution limits of species at the continental scale. Accordingly, it comprises a 28 year, hourly series of key above and below ground conditions for 1836 locations evenly sampled from ~5 km resolution interpolated daily weather data and ~90 m resolution estimated soil properties. Conditions are provided for four shade levels, allowing spatially implicit behavioural thermoregulation to be considered. Although based on a 5 km resolution climatology (adjusted to a 250 m resolution elevation grid), the model predicts the potential spatial variation at the cm scale in terms of vertical changes (height above surface, depth below ground) and horizontal changes (between different shade levels).

This article describes the data set and provides example analyses ranging from simple plotting of the raw data, to behaviourally-explicit calculations of animal activity, energy and water budgets.

Methods

The NicheMapR microclimate model, now completely open source https://github.com/mrke/NicheMapR, is described fully in Kearney and Porter (2017). Briefly, it comprises a first-principles solar radiation module, algorithms for hourly interpolation of vertical profiles of air temperature, wind speed and relative humidity, algorithms for computing terrain, cloud and vegetation shading influences on short- and longwave radiation streams, a full heat and water budget for the soil profile including a water infiltration model, and a coupled snow model. It requires as input the daily minima and maxima (or hourly observations if available) of air temperature, wind speed and relative humidity at a reference height, as well as cloud cover, substrate solar absorptivity and long-wave emissivity, soil thermal and hydraulic properties (depth-specific, including vegetation characteristics), and terrain characteristics (including elevation, slope, aspect, hill shade). It produces hourly output of the soil temperature, humidity, fractional moisture and water potential profiles, above ground air temperature, wind speed and relative humidity at a user-specified height, solar radiation and zenith angles, and sky temperature (accounting for cloud cover and shading) for determining down-welling longwave radiation.

To generate the microclimOz data set, the model, was run as described in Kearney and Maino (2018), from the years 1990 to 2017 inclusive across a grid of 1836 locations approximately 60 km apart. At each site, daily forcing data from the Australian Water Availability Project (AWAP) (Jones *et al.* 2009) on minimum and maximum air temperature, 9am and 3pm vapour pressure, total solar radiation and total precipitation was extracted, as well as 1.2 m wind speed from a daily gridded product (McVicar *et al.* 2008). It is important to note that the forcing air temperature, vapour pressure, precipitation and wind speed data are interpolations of weather station data. Minimum and maximum air temperatures were adjusted with respective lapse-rate corrections [0.0039 °C m^{-1} and 0.0077 °C m^{-1}, Ruddell et al. (1990)] from the 0.05° AWAP elevation grid to a 9 arc second DEM (Hutchinson *et al.* 2008), and depth-specific soil textural and density properties were extracted from the 3 arc second Soil and Landscape Grid of Australia (SLGA) data set (Viscarra Rossel *et al.* 2015, 2015) and converted to hydraulic properties with a pedotransfer function (Cosby *et al.* 1984) as described more fully in Kearney and Maino (2018). Flat ground was assumed. Substrate solar reflectivity was fixed at 0.15 and long-wave emissivity was extracted from a monthly 0.05° data set (Seemann *et al.* 2008) and splined to a daily time step. All the forcing data and terrain/soil variables for each location (minimum and maximum daily air temperature, minimum and maximum relative humidity, wind speed, rainfall, elevation, soil hydraulic properties), and the coordinates of the grid of 1836 points, are available in the data repository. For computations of solar radiation, an aerosol attenuation profile is required (McCullough and Porter 1971), which was based on data extracted for a single location from the eastern-most 5 degree resolution pixel of the Global Aerosol Data Set (GADS) (Koepke *et al.* 1997). All analyses were run in the statistical package R (R Development Core Team 2012).

Results and Discussion

The microclimOz data set is summarised in Table 1, and is available at https://knb.ecoinformatics.org/view/doi:10.5063/F15Q4T9Q. It comprises a series of netCDF files (each ~60 megabytes), a self-describing array-holding file format. Each file contains hourly values of a given variable for all 1836 locations evenly spaced ~60 km apart for each year (1990 – 2017) with the exception of the zenith angle outputs which are provided for a single leap and non-leap year. Most values have been multiplied by 10 and stored as integers to reduce file size. Shade-specific outputs are provided for 1cm air temperature, 1 cm relative humidity, sky temperature, snow depth, and for all soil outputs (temperature, moisture, water potential and humidity). The total data set comprises 4653 files and totals ~350 gigabytes representing over 74 billion hourly microclimate values.

The simulated microclimate data can be extracted for specific points or for selected grids, and the user can employ interpolation functions to obtain estimates at intermediate shade level or heights above the ground between 1cm and 120 cm if necessary. Interpolation of wind speed, *V*, and air temperature, *T*, between these two heights to any other height *z*, assuming neutral conditions (i.e. no strong free convection), can be achieved with the following equations (Sellers 1965)

$$V_z = (V^*/k)\ln\left(\frac{z}{z_0} + 1\right)$$

$$\frac{V_z}{V_r} = \frac{T_z - T_s}{T_r - T_s} = \frac{\ln\left(\frac{z}{z_0} + 1\right)}{\ln\left(\frac{z_r}{z_0} + 1\right)}$$

where V^* is the shear velocity (m s^{-1}), V_z is the wind speed at the new height, V_r is the reference wind speed, z_r is the reference height (m), z_0 is the assumed surface roughness (0.004 m in the present case), T_s is the surface temperature (°C), T_r is the air temperature a the reference height, T_z is the air temperature at the new height, and *k* is the Karman constant (0.4).

Some example plots and applications are provided below, with all the associated code and detailed explanations provided in the online supplement Appendix S1.

<u>Example output grids</u>

Figure 1a illustrates output grids for four different variables on the 1st January 2009. This includes the zenith angle of the sun, which is 0° when the sun is directly overhead and 90° when it is below the horizon. This variable is computed directly by the NicheMapR microclimate model following the equations in McCullogh and Porter (1971) and can be used to assess the times of sunrise and sunset, as well as the intensity of solar radiation in situations other than horizontal planes. In Figure 1 it can be seen that in early January the sun is most directly overhead around the tropic of Capricorn.

The solar radiation grid in Figure 1a shows high intensity solar radiation (> 1000 W m^{-2}) over much of Australia but cloud cover in the north-eastern regions has reduced the radiation levels substantially. The NicheMapR microclimate model computes clear sky solar radiation from first principals (McCullough and Porter 1971) but the results are then adjusted according to cloud cover which was inferred via the satellite-derived solar radiation from the AWAP data set.

The two other panels in Figure 1 show the wind speed and air temperature at 1 cm above the ground – a typical height for a small lizard, a large terrestrial insect, or a small forb. The wind speed at this height is strongly reduced by friction with the ground, and the air temperature at this time of the day is much higher than what would be measured by a weather station.

Example output time-series

Figure 2 shows some examples of hourly output extracted for the two locations indicated on the maps in Figure 1: near Old Andado Station in the Simpson Desert of the Northern Territory (Fig. 2a & b), and near Bendigo, Victoria (Fig. 2c & d), for 2009. Each file in the microclimOz data set comprises 8760 layers (non-leap years), one for each hour of the day, and such time series can be extracted for any of the 1836 locations. Appendix S1 (section 2) includes a function for extracting a time series of data for a given location.

It is clear from the air temperature plots in Figure 2a & c how much the 1cm air temperature differs from the 120 cm (weather station) air temperatures. Daily minimum and maximum air temperatures were used to generate the microclimates, with the internal daily interpolation algorithm of the NicheMapR microclimate model providing an estimate of the daily cycle. There was a major heat wave in 2009 in early February in southern Australia, which is evident for the Bendigo figures. Also note the substantial reduction in temperature variation with depth for the soil temperature plots (Fig. 2b & d).

Computing plant growth potential

Figure 3 provides an example time series plot of soil water potential, a metric which quantifies the ability of the soil to pull moisture out of e.g. a plant's roots or a lizard's eggs (water potential is for water flow like temperature is for heat flow - the steeper the gradient, the greater the flow). Water potential, which never rises above zero, is a function of both the soil moisture content and the texture (particle size, as dictated by the % sand, silt and clay). The more negative the water potential, the greater the pulling power. The microclimOz calculations used soil texture data extracted from the 90 m Soil and Landscape Grid of Australia for the nearest pixel to a given grid point. Grids of the actual soil hydraulic properties used (19 depth-specific values per site) are included in the data set.

Figure 3 shows soil water potential data at 10 cm depth as well as the results of a calculation of the cumulative summation of time above the permanent wilting point, assuming this to be -1500 J kg^{-1} (resetting whenever the wilting point is reached). It thus provides a prediction of cumulative plant growth potential, which should correlate with the greenness of vegetation having roots around 10 cm deep (this calculation could be extended by including a temperature dependence to growth). There is a stark contrast between the temperate and arid site.

Figure 4 shows the sums of the time above the permanent wilting point across all 8760 grids (i.e. hours of the year), thus providing an index of plant growth potential for 2009. Note the two patches of very low values in inland Western Australia - these are areas of very uncertain rainfall due to a dearth of weather stations, and are masked as zero in the AWAP data set.

Computing insect egg development

Soil temperature estimates are important for many applications, one being the estimation of insect egg development (Horton 2012). Figure 5 shows estimates of egg development for a native Australian matchstick grasshopper, *Warramaba virgo*. This grasshopper is univoltine, hatching in spring, living and feeding on shrubs (especially *Acacia*, *Senna*), and laying batches of eggs about 3 cm underground through the summer, as described in detail in Kearney *et al.* (2018). In Figure 5 its egg development is simulated at 5 cm depth assuming oviposition times of 0, 30 and 60 days from the start of the simulation (1st January). Note that at both sites some eggs would hatch before winter, but this does not happen in nature due to a summer diapause mechanism (Kearney, Deutscher, *et al.* 2018). Figure 6 shows the cumulative development time across all hours of 2009, indicating unsuitable conditions for egg development in coastal south-eastern Australia and Tasmania.

Computing ectotherm body temperature

Figure 7 provides an example of the use of the microclimOz data set to compute the heat budget of a lizard, based on the biology of the military dragon *Ctenophotus isolepis*. This lizard occurs in hummock grasslands (*Triodia*) on sand plains throughout inland Australia and forages in the open for ants (Losos 1987). The example results from computations of the potential body temperature of the lizard in either the 0% or 90% shade scenarios, using the voluntary foraging limits to choose between environments, i.e. to behaviourally thermoregulate. This example uses a very simplified heat budget model of a lizard provided in Gates (1980). The analysis indicates summertime constraints on foraging in open ground due to overheating in both locations, and predicts that the Bendigo location would preclude winter activity. Figure 8 illustrates the same calculations made across the whole spatial extent of the microclimOz data set at midday on 1st January 2009. The cloud cover indicated in Figure 1 is permitting cool enough conditions for activity in the north east of the country.

Computing endotherm metabolic heat and water requirements

In this final example, a heat budget is solved for an endotherm (mammal or bird) based on the equations of Porter and Kearney (2009) for an ellipsoid-shaped endotherm. This analytical solution, which is included in the NicheMapR package as function 'ellipsoid', is relevant for 'black body' radiation environments where the air and radiant temperatures are the same, as is approximated in a room, a house, a cave or very deep shade.

The 'ellipsoid' function finds the metabolic heat generation required to attain a specified core body temperature given the air temperature and wind speed of the environment and the size, shape and insulation (fur/feather depth and thermal conductivity) of the animal. The resulting solution may be above or below the basal metabolic rate for the animal in question. In the former case, a precise estimate is obtained of the additional energy expenditure required to for the animal to keep warm. In the latter case, an estimate is obtained of how much heat needs to be lost (typically through evaporation, via panting or sweating) to keep cool.

This particular example is based on a small rodent, the ash-grey mouse *Pseudomys albocinereus*, foraging under heavily shaded (90%) conditions or retreating to a 50 cm deep burrow. The physiology is based on Barker *et al.* (2012) who found the species to exhibit hyperthermia in hot conditions, allowing body temperature to rise to 37.8 ºC when air temperature rose above 34 ºC. A test of the ability of the model to capture laboratory observations is provided in Appendix S1. The analysis presented in Figure 9 incorporates changing behavioural states (posture, piloerection, hyperthermia) based on the experienced air temperature, as described fully in Appendix S1. Figure 10 shows the energy and water requirements predicted in 90% shade at the surface, on the same hour of the same day as used in the lizard analysis in Figure 7. The mouse is inferred to be significantly water stressed if restricted to the surface in the inland regions of Western Australia, losing up to 4% of their body mass in water per hour to remain cool.

Summary

The microclimOz data set provides the key microclimatic variables for computing the fundamental processes of heat and mass exchange between terrestrial organisms and their environments at the appropriate temporal resolution (hours). The calculated microclimatic conditions are based on the highest available spatial resolution in gridded meteorological and soil variables, and are provided a sufficient number of locations to provide a picture of factors potentially limiting the broad distributions of species. Because they are based on daily meteorological grids, they can be used to infer the effects of extreme conditions (Kearney *et al.* 2012; Briscoe *et al.* 2016; Morán-Ordóñez *et al.* 2017). Following preliminary analyses with the microclimOz data set, more targeted analyses (e.g. at different locations, higher resolution, different topographic settings, future climates) can be undertaken using the NicheMapR microclimate model directly (Kearney and Porter 2017).

The predictions incorporate a broad range of physical processes including interactions between heat and water flow through layered soil, buffering effects of snow, vertical gradients in air temperature, wind speed and relative humidity, based on fully physical equations. However, it must be born in mind there is no incorporation of local terrain effects (slope, aspect, hill shade) and the soil textural properties are drawn from the particular 90m resolution pixel for each point. With these limitations in mind, the data set should provide a way to rapidly compute a range of sophisticated metrics relating to the potential distribution and abundance of Australian organisms.

Acknowledgements

This work was supported by a resource allocation grant from the Victorian Life Sciences Computation Initiative (Melbourne Bioinformatics). I thank two anonymous reviewers for suggestions which significantly improved the manuscript.

References

Ashcroft M. B. & Gollan J. R. (2012) Fine-resolution (25 m) topoclimatic grids of near-surface (5 cm) extreme temperatures and humidities across various habitats in a large (200 × 300 km) and diverse region. *International Journal of Climatology* **32**, 2134–2148. doi: 10.1002/joc.2428

Barker J. M., Cooper C. E., Withers P. C. & Cruz-Neto A. P. (2012) Thermoregulation by an Australian murine rodent, the ash-grey mouse (*Pseudomys albocinereus*). *Comparative Biochemistry and Physiology Part A: Molecular & Integrative Physiology* **163**, 336–342. doi: 10.1016/j.cbpa.2012.07.011

Bennie J., Huntley B., Wiltshire A., Hill M. O. & Baxter R. (2008) Slope, aspect and climate: Spatially explicit and implicit models of topographic microclimate in chalk grassland. *Ecological Modelling* **216**, 47–59. doi: doi:10.1016/j.ecolmodel.2008.04.010

Bennie J., Wilson R. J., Maclean I. M. D. & Suggitt A. J. (2014) Seeing the woods for the trees - when is microclimate important in species distribution models? *Global Change Biology* **20**, 2699–2700. doi: 10.1111/gcb.12525

Bramer I., Anderson B. J., Bennie J. *et al.* (2018) Advances in Monitoring and Modelling Climate at Ecologically Relevant Scales. In: *Advances in Ecological Research* Elsevier. doi: 10.1016/bs.aecr.2017.12.005

Briscoe N. J., Kearney M. R., Taylor C. A. & Wintle B. A. (2016) Unpacking the mechanisms captured by a correlative species distribution model to improve predictions of climate refugia. *Global Change Biology* **22**, 2425–2439. doi: 10.1111/gcb.13280

Cosby B. J., Hornberger G. M., Clapp R. B. & Ginn T. R. (1984) A Statistical Exploration of the Relationships of Soil Moisture Characteristics to the Physical Properties of Soils. *Water Resources Research* **20**, 682–690. doi: 10.1029/WR020i006p00682

Gates D. M. (1980) *Biophysical Ecology*. Springer Verlag, New York.

Geiger R. (1950) *The Climate Near the Ground*. Harvard University Press, Cambridge, Mass.

Horton B. (2012) Models for estimation of hourly soil temperature at 5 cm depth and for degree-day accumulation from minimum and maximum soil temperature. *Soil Research* **50**, 447–454. doi: 10.1071/SR12165

Hutchinson M. F., Stein J. A., Stein J. L., Anderson H. & Tickle P. (2008) *Geodata 9 Second DEM and D8 - Digital Elevation Model Version 3 and Flow Direction Grid. User Guide*. Fenner School of Environment and Society, ANU and Geoscience Australia, Canberra.

Jones D., Wang W. & Fawcett R. (2009) High-quality spatial climate data-sets for Australia. *Australian Meteorological and Oceanographic Journal* **58**, 233–248. doi: 10.22499/2.5804.003

Kearney M. R. (2018) Microclimate Ecology. *Oxford Bibliographies*. doi: 10.1093/obo/9780199830060-0194 [online]. Available from: http://www.oxfordbibliographies.com/view/document/obo-9780199830060/obo-9780199830060-0194.xml [Accessed October 14, 2017].

Kearney M. R., Deutscher J., Kong J. D. & Hoffmann A. A. (2018) Summer egg diapause in a matchstick grasshopper synchronizes the life cycle and buffers thermal extremes. *Integrative Zoology* **13**, 437–449. doi: 10.1111/1749-4877.12314

Kearney M. R., Isaac A. P. & Porter W. P. (2014) microclim: Global estimates of hourly microclimate based on long-term monthly climate averages. *Scientific Data*. doi: doi: 10.1038/sdata.2014.6

Kearney M. R. & Maino J. L. (2018) Can next-generation soil data products improve soil moisture modelling at the continental scale? An assessment using a new microclimate package for the R programming environment. *Journal of Hydrology*. doi: 10.1016/j.jhydrol.2018.04.040

Kearney M. R., Matzelle A. & Helmuth B. (2012) Biomechanics meets the ecological niche: the importance of temporal data resolution. *The Journal of Experimental Biology* **215**, 922–933. doi: 10.1242/jeb.059634

Kearney M. R., Munns S. L., Moore D., Malishev M. & Bull C. M. (2018) Field tests of a general ectotherm niche model show how water can limit lizard activity and distribution. *Ecological Monographs* **0**. doi: 10.1002/ecm.1326

Kearney M. R. & Porter W. P. (2017) NicheMapR - an R package for biophysical modelling: the microclimate model. *Ecography* **40**, 664–674. doi: 10.1111/ecog.02360

Kearney M. R., Shamakhy A., Tingley R. *et al.* (2014) Microclimate modelling at macro scales: a test of a general microclimate model integrated with gridded continental-scale soil and weather data. *Methods in Ecology and Evolution*. doi: doi: 10.1111/2041-210X.12148

Koepke P., Hess M., Schult I. & Shettle E. P. (1997) *Global Aerosol Data Set*. Max-Planck-Institut für Meteorologie, Hamburg.

Levy O., Buckley L. B., Keitt T. H. & Angilletta M. J. (2016) A dynamically downscaled projection of past and future microclimates. *Ecology* **97**, 1888–1888. doi: 10.1002/ecy.1444

Losos J. B. (1987) Postures of the Military Dragon (Ctenophorus isolepis) in relation to substrate temperature. *Amphibia Reptilia*.

Maclean I. M. D., Mosedale J. R. & Bennie J. J. (2018) Microclima: an R package for modelling meso- and microclimate. *Methods in Ecology and Evolution*. doi: 10.1111/2041-210X.13093

McCullough E. C. & Porter W. P. (1971) Computing clear day solar radiation spectra for the terrestrial ecological environment. *Ecology* **52**, 1008–1015. doi: 10.2307/1933806

McVicar T. R., Van Niel T. G., Li L. T. *et al.* (2008) Wind speed climatology and trends for Australia, 1975-2006: Capturing the stilling phenomenon and comparison with near-surface reanalysis output. *Geophysical Research Letters* **35**, L20403. doi: 10.1029/2008GL035627

Morán-Ordóñez A., Briscoe N. J. & Wintle B. A. (2017) Modelling species responses to extreme weather provides new insights into constraints on range and likely climate change impacts for Australian mammals. *Ecography*. doi: 10.1111/ecog.02850

Porter W. P. & Gates D. M. (1969) Thermodynamic equilibria of animals with environment. *Ecological Monographs* **39**, 227–244. doi: 10.2307/1948545

Porter W. P. & Kearney M. (2009) Size, shape, and the thermal niche of endotherms. *Proceedings of the National Academy of Sciences* **106**, 19666–19672. doi: 10.1073/pnas.0907321106

R Development Core Team (2012) R: A language and environment for statistical computing. R Foundation for Statistical Computing, Vienna, Austria. ISBN 3-900051-07-0, URL http://www.R-project.org/.

Ruddell A. R., Budd W. F., Smith I. N., Keage P. L. & Jones R. (1990) *The south east Australian alpine climate study*. The University of Melbouren and the Department of Meteorology an Alpine Resorts Comission, Victoria, Melboure, Victoria.

Seemann S. W., Borbas E. E., Knuteson R. O., Stephenson G. R. & Huang H.-L. (2008) Development of a Global Infrared Land Surface Emissivity Database for Application to Clear Sky Sounding Retrievals from Multispectral Satellite Radiance Measurements. *Journal of Applied Meteorology and Climatology* **47**, 108–123. doi: 10.1175/2007jamc1590.1

Sellers W. D. (1965) *Physical Climatology*. University of Chicago Press, Chicago.

Varner J. & Dearing M. D. (2014) The importance of biologically relevant microclimates in habitat suitability assessments. *PLOS ONE* **9**, e104648. doi: 10.1371/journal.pone.0104648

Viscarra Rossel R. A., Chen C., Grundy M. J., Searle R., Clifford D. & Campbell P. H. (2015) The Australian three-dimensional soil grid: Australia's contribution to the GlobalSoilMap project. *Soil Research* **53**, 845–864. doi: 10.1071/SR14366

Table 1. The microclimOz data sets, each containing grids of hourly values for one year. For the naming convention, the part in italics denotes the particular scenario as follows: *year* is the year simulated (1990 to 2017), *sh* is shade level in % (0, 50, 70, 90), *depth* is depth in cm below ground (0, 2.5, 5, 10, 15, 20, 30, 50, 100 & 200 cm).

variable	units	sublevels	naming convention	example
solar zenith angle	degrees	-	ZEN.nc or ZEN_leap.nc	ZEN.nc (solar zenith angles for non-leap years)
solar radiation	W m^{-2}	*year*	SOLR_*year*.nc	SOLR_1990.nc (solar radiation for 1990)
sky radiant temperature	°C	*year*, *shd*	TSKYC_*sh*pctShade_ *year*.nc	TSKYC_50pctShade_1990.nc (sky radiant temp. for 50% shade, 1990)
air temp. at 120 cm	°C	*year*	TA120cm_ *year*.nc	TA120cm_1990.nc (air temp. at 120 cm for January)
air temp. at 1cm	°C	*year*, *shd*	TA1cm_ *sh*pctShade _ *year*.nc	TA1cm_rock_50_1990.nc (air temp. at 1cm for 50% shade for 1990)
wind speed at 10 m	m s^{-1}	*year*	V120cm_ *year*.nc	V10m_1990.nc (wind speed at 10m for January)
wind speed at 1cm	m s^{-1}	*year*	V1cm_ *year*.nc	V1cm_1990.nc (wind speed at 1cm for January)

relative humidity at 1.2 m	%	*year*	RH120cm_ *year*.nc	RH120cm_1990.nc (relative humidity at 120cm for January)
relative humidity at 1cm	%	*year*, *shd*	RH1cm_ *sh*pctShade _ *year*.nc	RH1cm_50_1990.nc (relative humidity at 1cm for sand substrate and 50% shade for January)
snow depth	cm	*year*, *shd*, *depth*	SNOWDEP_ *sh*pctShade _ *year*.nc	SNOWDEP_50_1990.nc (snow depth for 50% shade 1990)
soil temperature at specific depths	°C	*year*, *shd*, *depth*	soil*depth*cm_ *sh*pctShade _ *year*.nc	soil5cm_50_1990.nc (substrate temperature at 5 cm depth for 50% shade 1990)
soil water potential specific depths	J kg^{-1}	*year*, *shd*, *depth*	pot*depth*cm_ *sh*pctShade _ *year*.nc	pot5cm_50_1990.nc (soil water potential at 5 cm depth for 50% shade 1990)
soil moisture at specific depths	%	*year*, *shd*, *depth*	moist*depth*cm_ *sh*pctShade _ *year*.nc	moist5cm_50_1990.nc (soil moisture at 5 cm depth for 50% shade 1990)
soil humidity at specific depths	%	*year*, *shd*, *depth*	humid*depth*cm_ *sh*pctShade _ *year*.nc	humid5cm_50_1990.nc (soil humidity at 5 cm depth for 50% shade 1990)

Figure 1. Example mapped outputs of a) solar zenith angle, b) horizontal plane solar radiation, c) 1 cm wind speed and d) 1 cm air temperature (0% shade) extracted from the microclimOZ data set for a particular hour. The two black dots indicate the sites for which example time series are extracted in Figs. 2, 3, 5, 7 & 9.

Figure 2. Hourly trajectories of 1 cm and 120 cm air temperature (a, c) and 0 cm, 5 cm and 50 cm soil temperature (b, d) extracted for two sites for the year 2009 under 0% shade. The site locations are indicated in Figure 1.

Figure 3. Hourly soil water potential estimates from the microclimOz data set for 2009 (0% shade) at two locations (a, c) and associated estimates of cumulative growth potential (b, d) based on time above the permanent wilting point (PWP) of -1500 J/kg.

Figure 4. Summation for 2009 of cumulative time spent above the permanent wilting point (-1500 J kg^{-1}) based on microclimOz estimated 10 cm soil water potential (0% shade).

Figure 5. Development rate of the matchstick grasshopper *Warramaba virgo* estimated from microclimOz estimated 5 cm soil temperature (0% shade) at two sites in 2009 (a, c) and cumulative developmental completions assuming oviposition dates days 1, 30 and 60 of that year (b, d).

Figure 6. Cumulative development of the matchstick grasshopper *Warramaba virgo* estimated over the year 2009 based on microclimOz soil temperature estimates at 5 cm (0% shade).

Figure 7. Estimates of potential body temperature (a, c), and activity time (b, d) for the military dragon *Ctenophorus isolepis* at two locations in 2009. Estimated body temperature in panels a & c includes that expected if the lizard stayed in full sun (Tb_sun), in full shade shade (Tb_shade), as well as the final body temperature after a thermoregulation algorithm is applied (Tb_treg). Gaps along horizontal hourly lines indicate when daytime activity in the sun is not thermally possible. These calculations are based on a simple biophysical model of heat exchange for a lizard (Gates 1980, p.349) and driven by microclimOz estimates of solar radiation, 1 cm air temperature, soil surface temperature, sky radiant temperature, 1 cm wind speed and solar zenith angle under 0% and 90% shade. Daytime shade requirements are also indicated (dark green vertical lines in a, c), with activity assumed to occur only in the open.

Figure 8. Estimates of a) potential body temperature in the open, b) activity state (green = active), c) body temperature after thermoregulation, and d) shade required (green = in shade) for the military dragon *Ctenophorus isolepis* at midday on 1st January 2009. These calculations are based on a simple biophysical model of heat exchange for a lizard (Gates 1980, p.349) and driven by microclimOz estimates of solar radiation, 1 cm air temperature, soil surface temperature, sky radiant temperature, 1 cm wind speed and solar zenith angle under 0% and 90% shade.

Figure 9. Estimated energy requirements (multiplicative increase on basal metabolic rate) and water requirements (% of hydrated body mass lost per hour) for the ash-grey mouse *Pseudomys albocinereus* at two depths (on the surface and in a burrow at 50 cm) and two locations in 2009. These calculations are based on a simple ellipsoid model of heat exchange for an endotherm (Porter and Kearney 2009) and driven by microclimOz estimates of either

air temperature, wind speed and relative humidity at 1 cm (90% shade), or 50 cm soil temperature (assuming 0.1 m s^{-1} wind speed and 100% relative humidity).

Figure 10. Estimated energy requirements (a & b) and water requirements (c & d) for the ash-grey mouse *Pseudomys albocinereus* in deep (90%) shade on the surface at midday on 1st January 2009. These calculations are based on a simple ellipsoid model of heat exchange for an endotherm (Porter and Kearney 2009) and driven by microclimOz estimates of 1 cm air temperature (90% shade), 1 cm wind and relative humidity. The sudden drops in metabolic rate, which are particularly apparent in the burrow simulations, represent simulation of torpor (see Appendix I).

Figure 1.

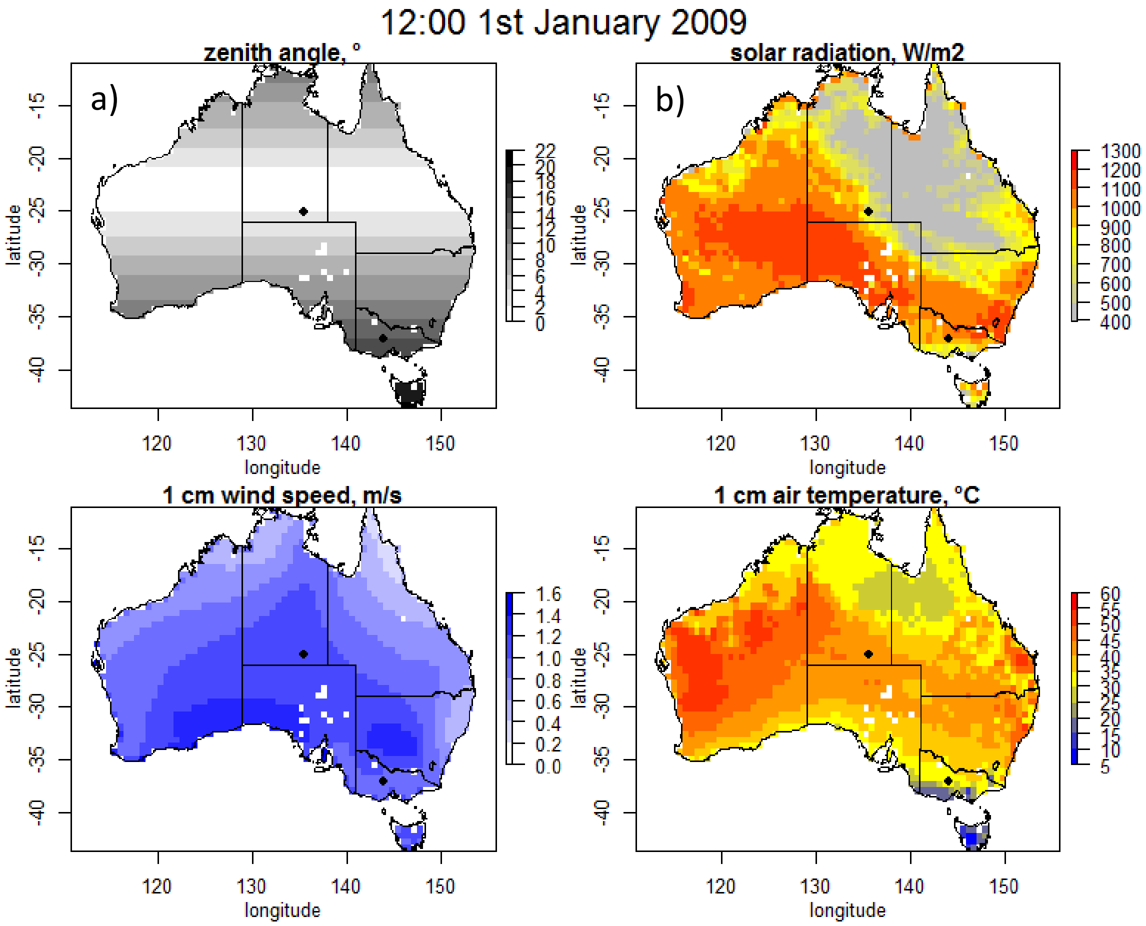

12:00 1st January 2009
zenith angle, °
a)
solar radiation, W/m2
b)
1 cm wind speed, m/s
1 cm air temperature, °C
latitude
longitude

Figure 2.

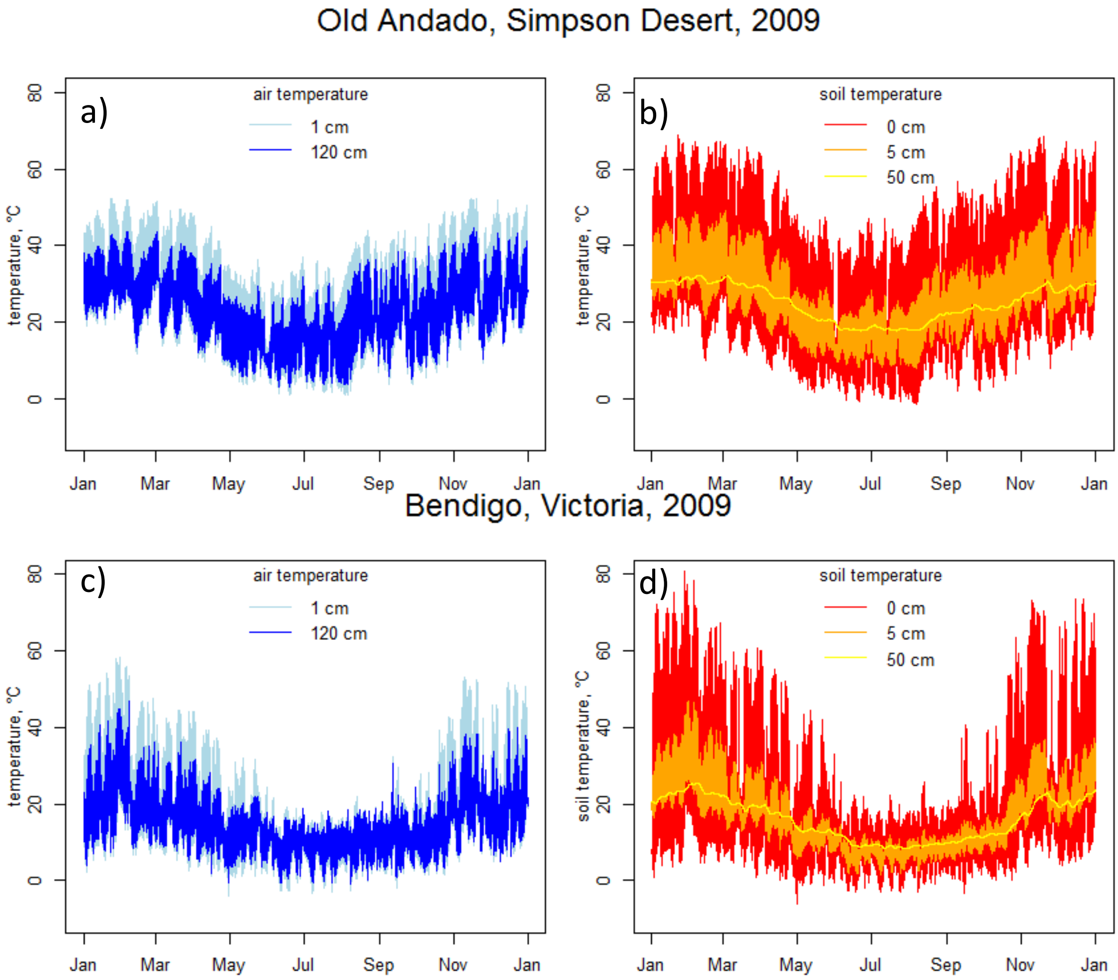

Old Andado, Simpson Desert, 2009
a)
air temperature
1 cm
120 cm
temperature, °C
0
20
40
60
80
Jan
Mar
May
Jul
Sep
Nov
Jan
b)
soil temperature
0 cm
5 cm
50 cm
temperature, °C
Bendigo, Victoria, 2009
c)
air temperature
1 cm
120 cm
temperature, °C
d)
soil temperature
0 cm
5 cm
50 cm
soil temperature, °C

Figure 3.

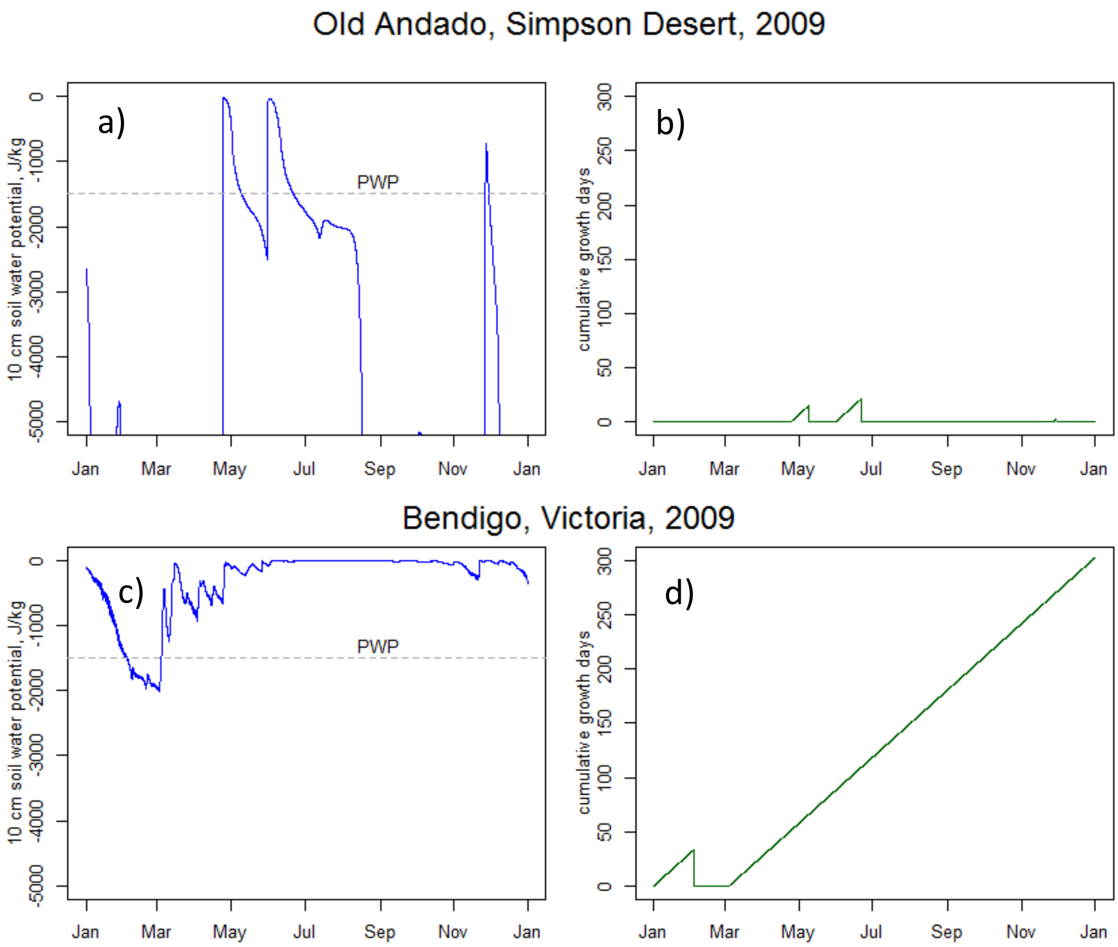
Old Andado, Simpson Desert, 2009
a)
b)
PWP
10 cm soil water potential, J/kg
cumulative growth days
Bendigo, Victoria, 2009
c)
d)
Jan
Mar
May
Jul
Sep
Nov
0
-1000
-2000
-3000
-4000
-5000
0
50
100
150
200
250
300

Figure 4.

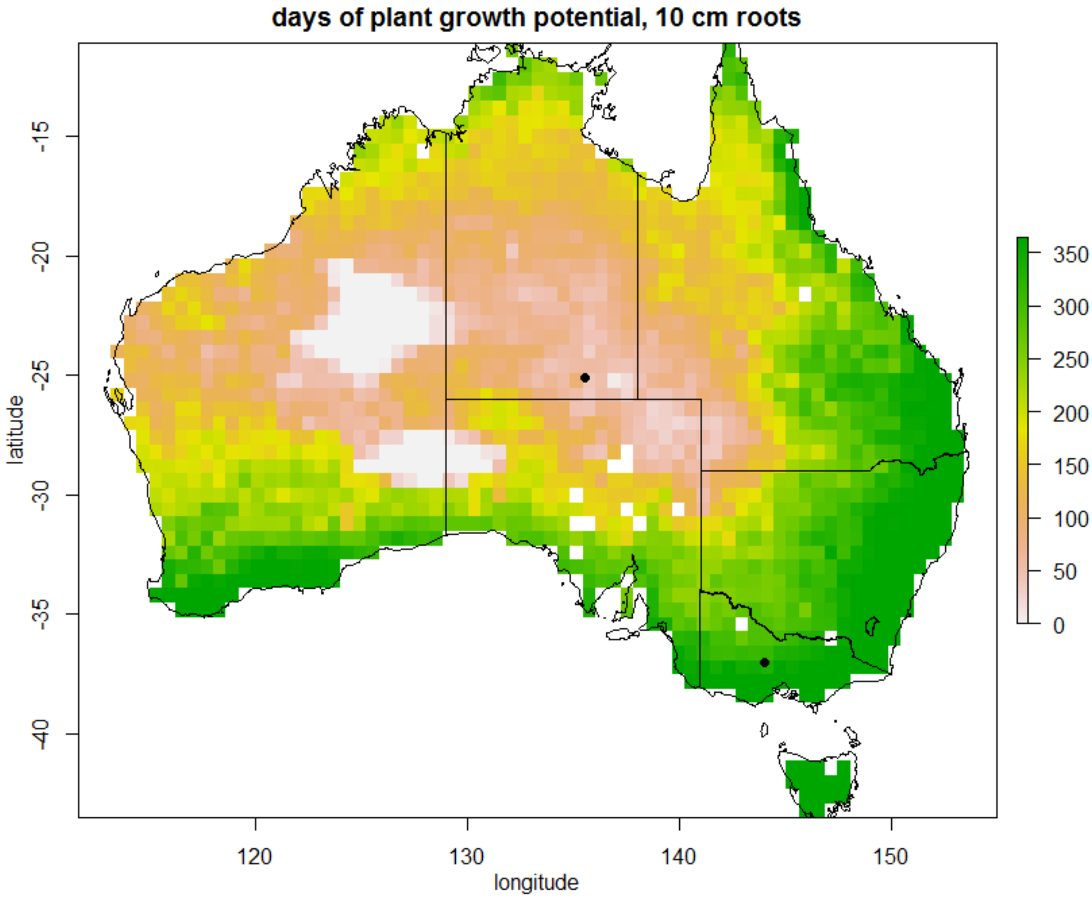
days of plant growth potential, 10 cm roots
latitude
-15
-20
-25
-30
-35
-40
longitude
120
130
140
150
350
300
250
200
150
100
50
0

Figure 5.

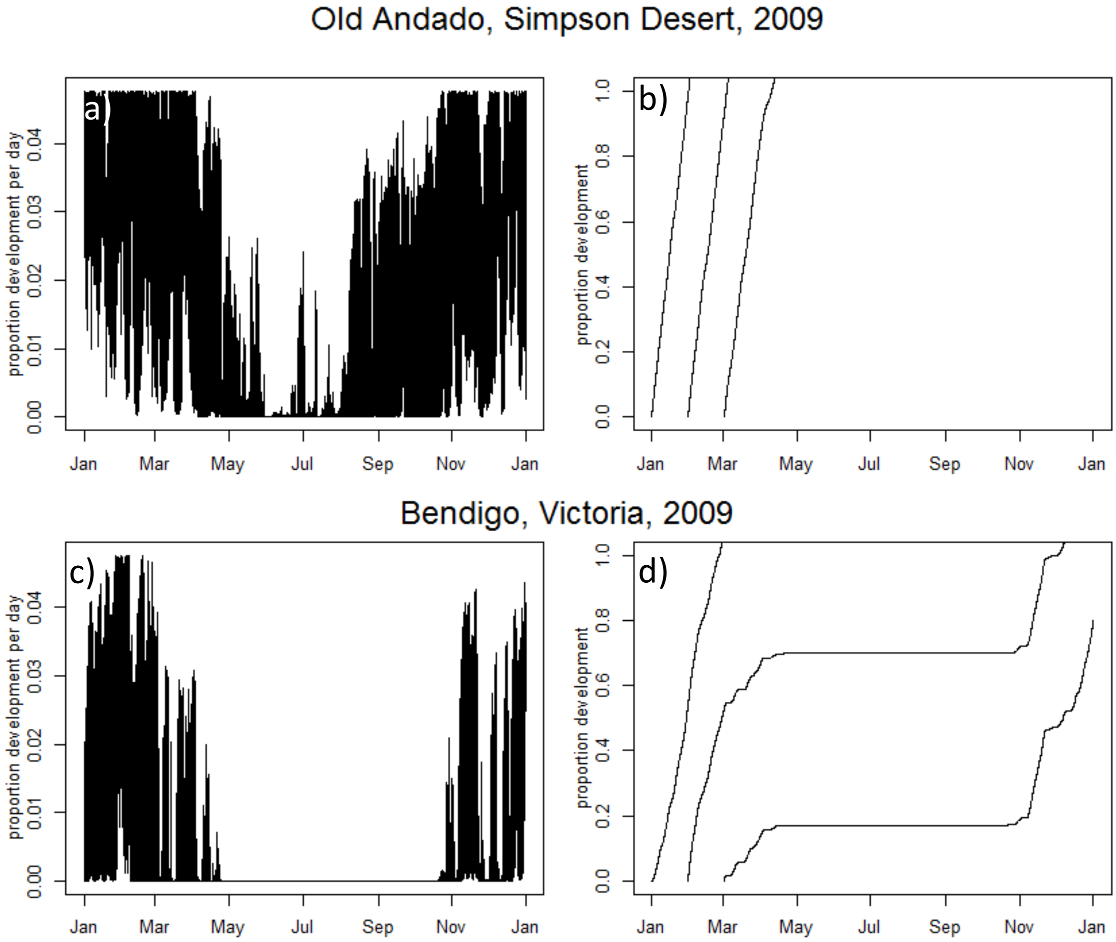

Old Andado, Simpson Desert, 2009
a)
b)
Bendigo, Victoria, 2009
c)
d)
proportion development per day
proportion development
0.00
0.01
0.02
0.03
0.04
0.0
0.2
0.4
0.6
0.8
1.0
Jan
Mar
May
Jul
Sep
Nov
Jan

Figure 6.

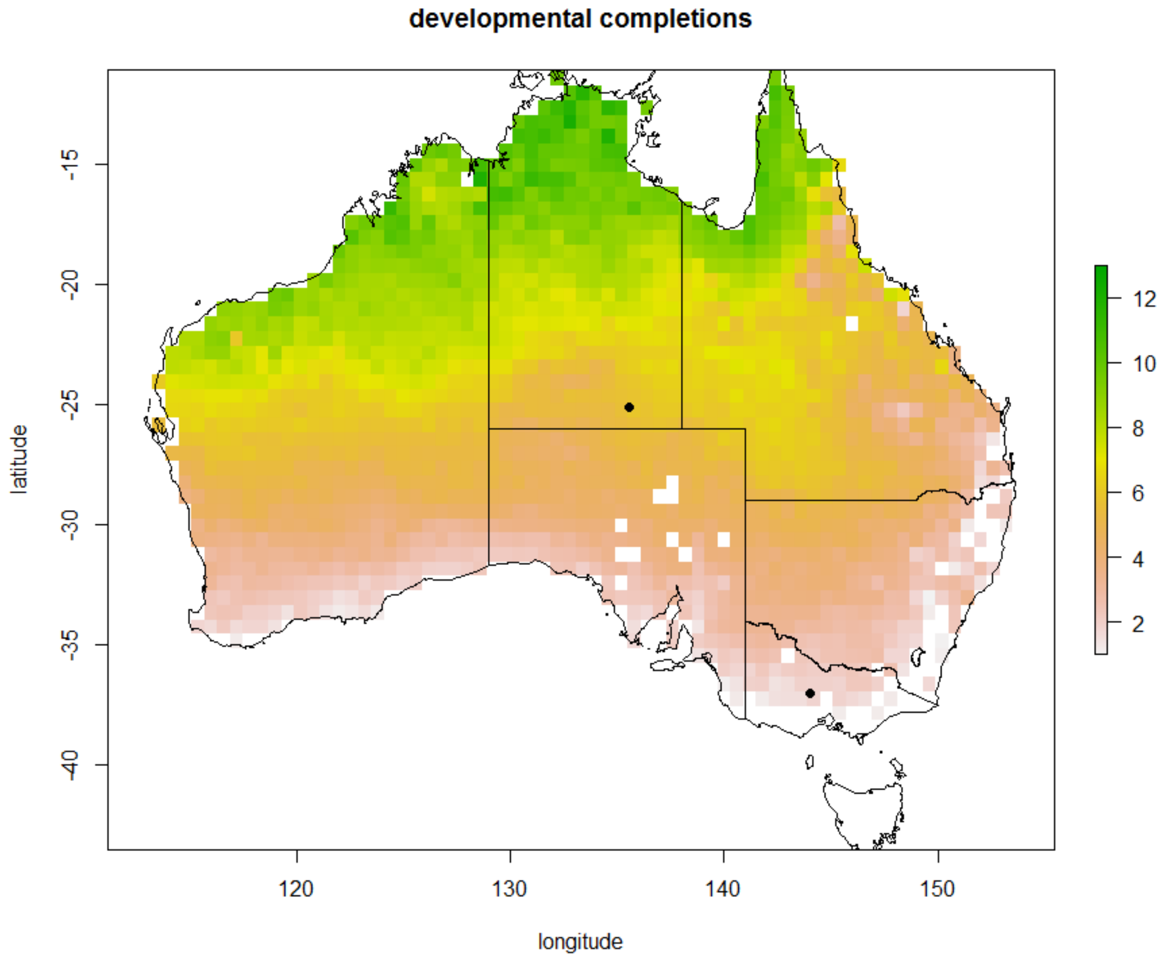

developmental completions
latitude
-15
-20
-25
-30
-35
-40
longitude
120
130
140
150
12
10
8
6
4
2

Figure 7.

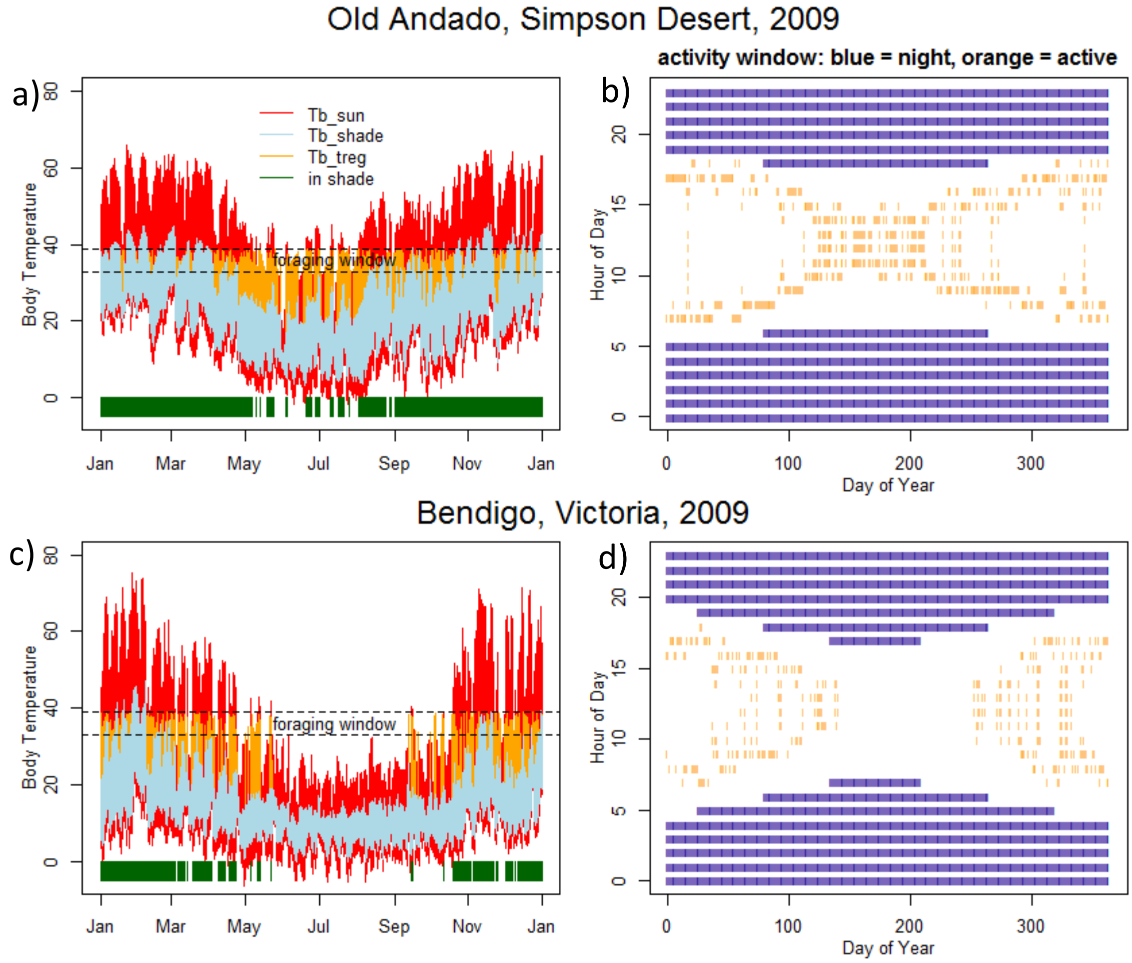

Old Andado, Simpson Desert, 2009
a)
Body Temperature
Tb_sun
Tb_shade
Tb_treg
in shade
foraging window
Jan
Mar
May
Jul
Sep
Nov
Jan
b)
activity window: blue = night, orange = active
Hour of Day
Day of Year
Bendigo, Victoria, 2009
c)
Body Temperature
foraging window
d)
Hour of Day
Day of Year

Figure 8.

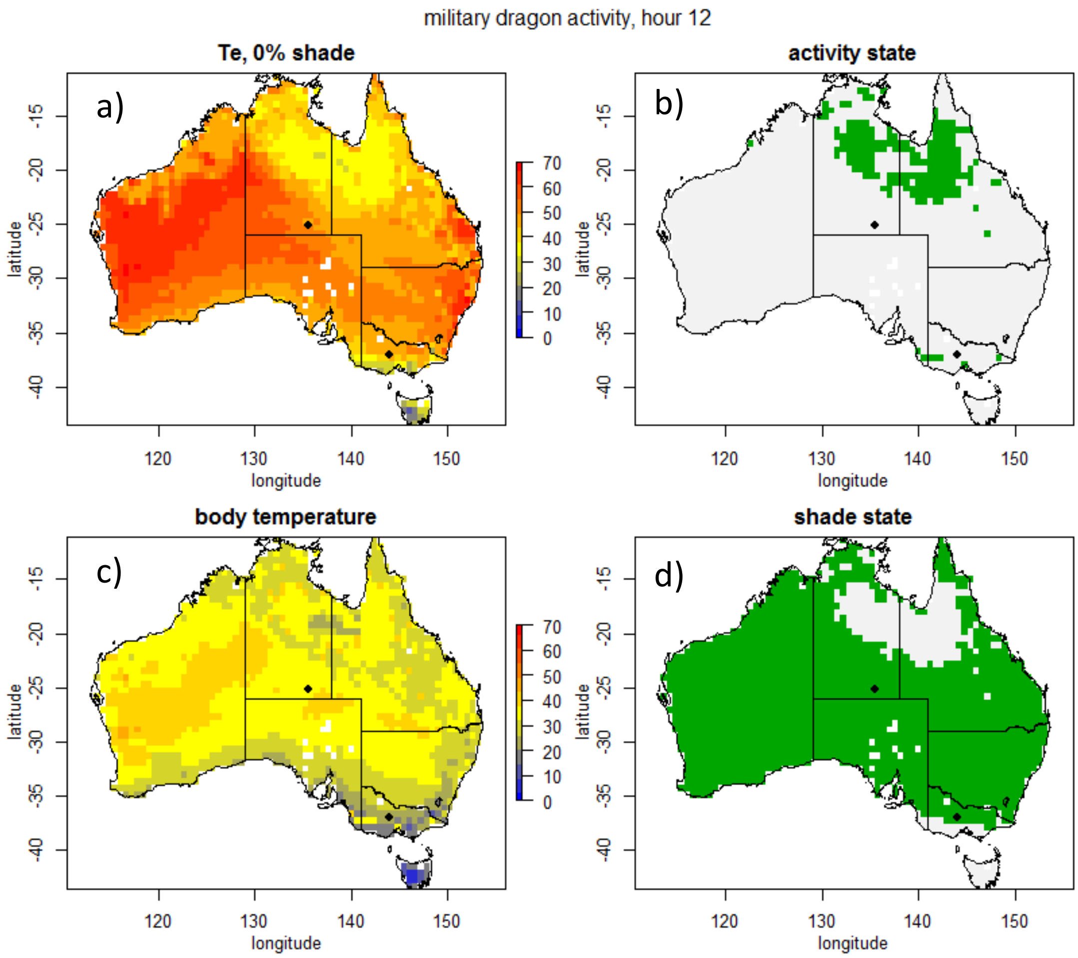

military dragon activity, hour 12
Te, 0% shade
a)
activity state
b)
body temperature
c)
shade state
d)
latitude
longitude
-15
-20
-25
-30
-35
-40
120
130
140
150
70
60
50
40
30
20
10
0

Figure 9.

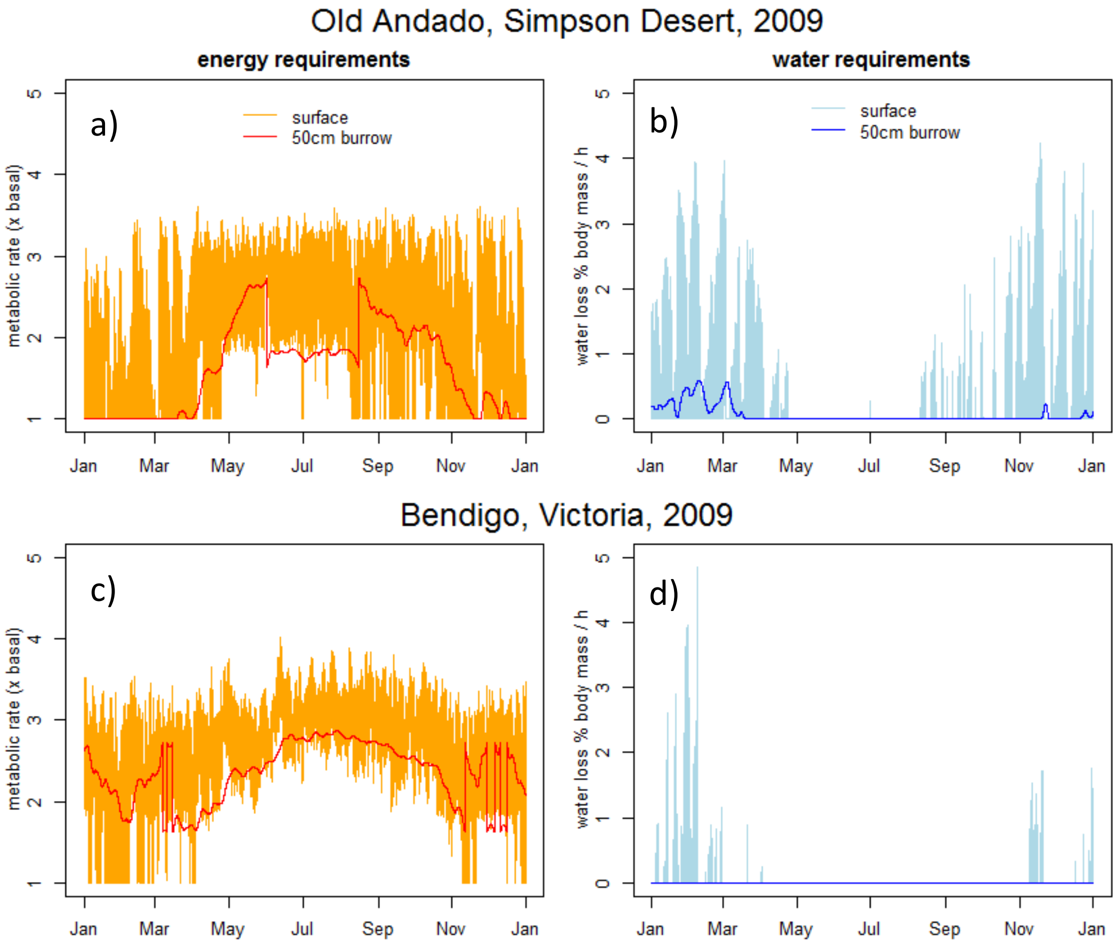

Old Andado, Simpson Desert, 2009
energy requirements
water requirements
a)
surface
50cm burrow
metabolic rate (x basal)
b)
surface
50cm burrow
water loss % body mass / h
Jan
Mar
May
Jul
Sep
Nov
Jan
Bendigo, Victoria, 2009
c)
d)

Figure 10.

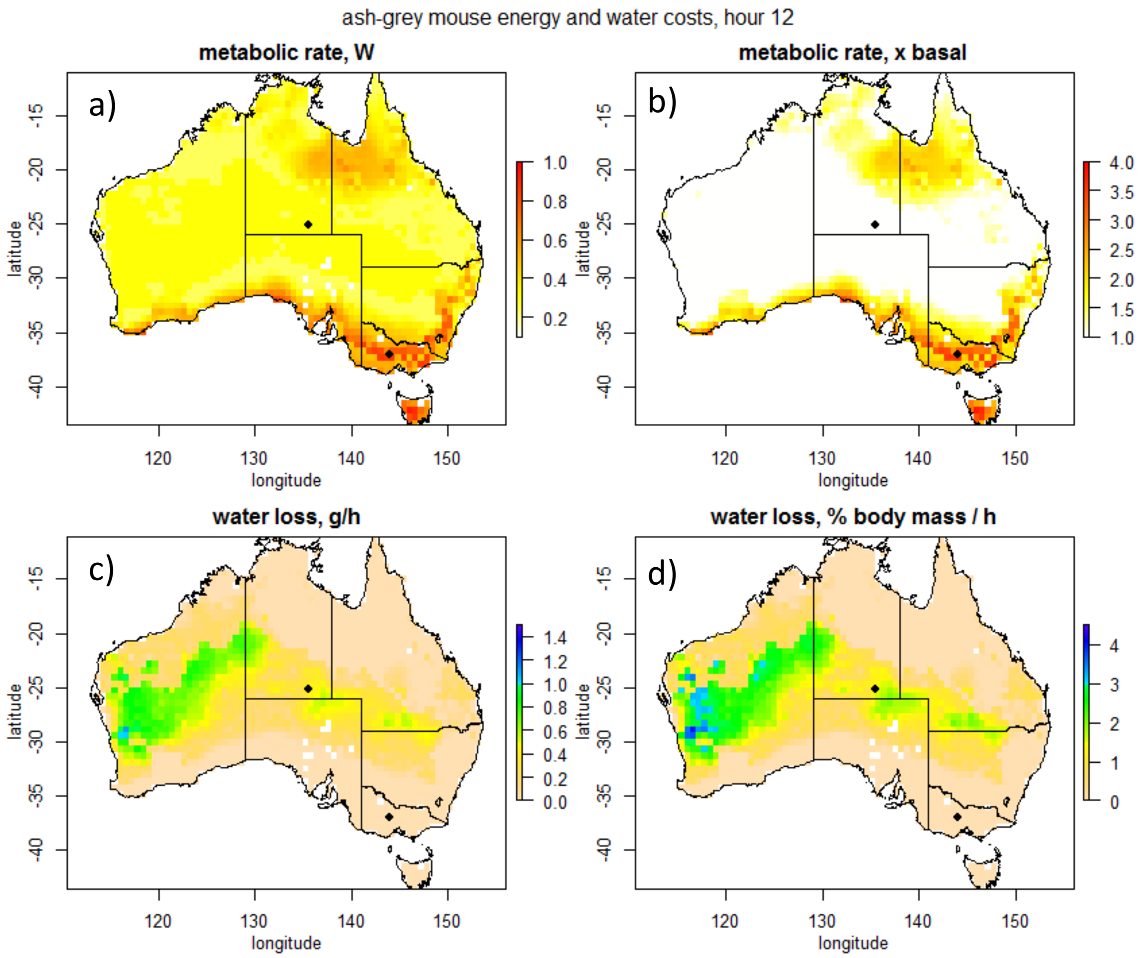

ash-grey mouse energy and water costs, hour 12
metabolic rate, W
a)
metabolic rate, x basal
b)
water loss, g/h
c)
water loss, % body mass / h
d)
latitude
longitude